Stem Cell Research 30 (2018) 130–140

Contents lists available at ScienceDirect

Stem Cell Research

journal homepage: www.elsevier.com/locate/scr

iPSC-derived neurons of *CREBBP*- and *EP300*-mutated Rubinstein-Taybi syndrome patients show morphological alterations and hypoexcitability

Valentina Alari[a,1], Silvia Russo[a,1], Benedetta Terragni[b], Paola Francesca Ajmone[c], Alessandra Sironi[a], Ilaria Catusi[a], Luciano Calzari[a], Daniela Concolino[d], Rosa Marotta[d], Donatella Milani[e], Daniela Giardino[a], Massimo Mantegazza[b,f,g], Cristina Gervasini[h], Palma Finelli[a], Lidia Larizza[a,*]

[a] Laboratory of Medical Cytogenetics and Molecular Genetics, Centro di Ricerche e Tecnologie Biomediche, IRCCS Istituto Auxologico Italiano, 20145 Milano, Italy
[b] Dept. of Neurophysiology and Diagnostic Epileptology, IRCCS Foundation C. Besta Neurological Institute, 20133 Milano, Italy
[c] Child and Adolescent Neuropsychiatric Service (UONPIA), Fondazione IRCCS Ca' Granda Ospedale Maggiore Policlinico, 20122 Milano, Italy
[d] Pediatrics Unit, Department of Medical and Surgical Science, University "Magna Graecia", 88100 Catanzaro, Italy
[e] Pediatric Highly Intensive Care Unit, Fondazione IRCCS Ca' Granda Ospedale Maggiore Policlinico, 20122 Milano, Italy
[f] Institute of Molecular and Cellular Pharmacology (IPMC), CNRS UMR7275, LabEx ICST, 06560 Valbonne-Sophia Antipolis, France
[g] Université Côte d'Azur (UCA), 06560 Valbonne-Sophia Antipolis, France
[h] Medical Genetics, Department of Health Sciences, Università degli Studi di Milano, 20142 Milano, Italy

ARTICLE INFO

Keywords:
Rubinstein-Taybi syndrome
Cognitive impairment
iPSCs
Neuronal model
Disease-relevant cell phenotypes

ABSTRACT

Rubinstein-Taybi syndrome (RSTS) is a rare neurodevelopmental disorder characterized by distinctive facial features, growth retardation, broad thumbs and toes and mild to severe intellectual disability, caused by heterozygous mutations in either *CREBBP* or *EP300* genes, encoding the homologous CBP and p300 lysine-acetyltransferases and transcriptional coactivators. No RSTS in vitro induced Pluripotent Stem Cell (iPSC)-neuronal model is available yet to achieve mechanistic insights on cognitive impairment of RSTS patients. We established iPSC-derived neurons (i-neurons) from peripheral blood cells of three *CREBBP*- and two *EP300*-mutated patients displaying different levels of intellectual disability, and four unaffected controls. Pan neuronal and cortical-specific markers were expressed by all patients' i-neurons. Altered morphology of patients' differentiating neurons, showing reduced branch length and increased branch number, and hypoexcitability of differentiated neurons emerged as potential disease biomarkers. Anomalous neuronal morphology and reduced excitability varied across different RSTS patients' i-neurons. Further studies are needed to validate these markers and assess whether they reflect cognitive and behavioural impairment of the donor patients.

1. Introduction

Rubinstein-Taybi syndrome (RSTS1 MIM 180849, RSTS2 MIM 613684) is a very rare (1: 125.000) autosomal dominant disorder characterized by distinctive facial dysmorphisms (mainly downslanting palpebral fissures, broad nasal bridge/beaked nose, columella below the alae nasi, microcephaly) skeletal anomalies, including the diagnostic sign of broad/short thumbs and/or big toes, mild-to-severe intellectual disability (ID), multiple organ anomalies and increased cancer risk (Hennekam, 2006). Heterozygous de novo mutations in either of the two highly conserved *CREBBP* or *EP300* genes, encoding the CBP and p300 histone and non-histone lysine acetyltransferases, acting in chromatin remodelling and transcriptional activation, account for 55% and 8% of clinically diagnosed patients, respectively (Spena et al., 2015; Negri et al., 2016). Like other developmental disorders with intellectual disability (DD/ID) caused by genes of the "epigenetic machinery" (Bjornsson, 2015) RSTS is characterized by wide phenotypic breadth, although the clinical presentation including cognitive impairment is globally milder in RSTS2 than in RSTS1 patients (Negri et al., 2016; Fergelot et al., 2016). Besides the affected locus, the site and type of mutation are strong determinants of the variable overall phenotype and intellectual disability which represents the most common and handicapping sign across and within *CREBBP* and *EP300*-mutated patients. Most pathogenic variants in both causative genes are inactivating (frameshift, nonsense, splice-site) and are predicted to exert their effect by a loss of function mechanism leading to

* Corresponding author.
E-mail address: l.larizza@auxologico.it (L. Larizza).
[1] Equal Contribution.

https://doi.org/10.1016/j.scr.2018.05.019
Received 11 December 2017; Received in revised form 9 May 2018; Accepted 29 May 2018
Available online 30 May 2018

haploinsufficiency, though dominant negative inhibition of wild type allele by putative truncating variants has been also proposed (Park et al., 2014). As regards missense variants, rare in *EP300*, those mainly clustered in *CREBBP* exons encoding the lysine (K) acetyltransferase (KAT) domain, are shown to encode proteins defective in the key catalytic function. Conversely a gain of function mechanism has been hypothesized for missense mutations in parts of *CREBBP* exons 31–32 and homologous *EP300* regions affecting the proper conformation of zinc fingers domains. Patients carrying these variants manifest a phenotype distinct from the classic one (Menke et al., 2018), consistent with the huge RSTS phenotypic variability.

Notwithstanding the generation of patient-specific iPSCs neurons has been an increasingly used tool to dissect the etiology of neurodevelopmental disorders (Chamberlain, 2016; Ardhanareeswaran et al., 2017), no iPSC modeling has been developed for RSTS to date. We selected from our wide cohort of molecularly characterized *CREBBP*- and *EP300*-mutated patients cases representative of different levels of intellectual impairment to generate, along with unaffected controls, iPSCs-derived neurons. We herein present data on the successful reprogramming to iPSCs of blood cells of four RSTS1 and two RSTS2 cases and the obtainment of neuronal derivatives in all cases. Characterization of i-neurons from five patients shows that RSTS i-neurons display, by cellular morphology and electrophysiology, a number of differences, as compared to controls, which attest impairment, variable across patients, of the proper differentiation program.

2. Materials and methods

2.1. Ethic issues

This study was approved by the Institutional ethical committee of IRCCS Istituto Auxologico Italiano, Milan. Written informed consent was obtained from all patients' parents and control individuals.

2.2. Selection of RSTS patients for iPSC reprogramming

Six patients were selected for iPSC modeling based on their availability for the study from previously clinically and molecularly characterized RSTS1 and RSTS2 patients and named with their original code (#34, #46, #149, #158 and #65, #207). The clinical description and molecular characterization of *CREBBP*-mutated patients #34, #46, #149 and #158 can be found in Bentivegna et al., 2006, Lopez-Atalaya et al., 2012 and Spena et al., 2015, and of *EP300*-mutated patients #65 and #207 in Negri et al., 2016.

Four control individuals were selected for iPSCs reprogramming. C1 and C2 are adult healthy females aged 51 and 40 at the time of withdrawal: C2 is the mother of patient #149. C3 and C4 are pediatric controls, aged 16 and 4 at the time of withdrawal: C3 is the healthy brother of patient #34 and C4 is the healthy sister of a patient affected by Angelman syndrome.

2.3. Neuropsychiatric assessment of RSTS patients

To assess Intellectual Quotient (IQ) the Leiter International Performance Scales Revised – Leiter-R (age range 2–21) was used (Roid and Miller, 1997), for its nonverbal characteristics and the availability of a brief form. A brief IQ in fact can be obtained, even if the patients show significant attention and communication difficulties. To assess the General Quotient of Development (GQ) the Griffiths' scale (Griffiths, 1986) which gives a GQ in patients from 0 to 8 years old, was used.

The behavioural characteristics of the patients were assessed using the Child Behaviour Checklist-CBCL 1.5–5 and 6–18 forms (Achenbach and Rescorla, 2001). The CBCL is a questionnaire about the behavioural characteristics of the child filled in by the parents. Each item is rated from 0 to 2. Internalizing, Total and Externalizing problems scales and 6 DSM IV oriented scales are obtained by the items score. We used the Social Communication Questionnaire: Lifetime Version SCQ (Rutter et al., 2003; Berument et al., 1999) to assess Autism spectrum disorders (ASD). The SCQ is a 40 item informant screening questionnaire for the presence of ASD in people with IDs. The SCQ was shown to have good concurrent validity with the Autism Diagnostic Observation Schedule (ADOS) and Autism Diagnostic Interview (ADI) (Berument et al., 1999; Howlin and Karpf, 2004).

2.4. Generation and culture of iPSCs

iPSCs were generated from Peripheral Blood Mononuclear Cells (PBMCs) of RSTS patients and healthy controls as described (Dowey et al., 2012). Cells were transduced with integration-free Sendai virus kit (CytoTune 2.0,Thermo Fisher Scientific Waltham, MA, USA) and grown on MEF (Mouse Embryonic Fibroblast) feeder layer in human embryonic stem cell medium (DMEM-F12, 20% knockout serum replacement, 1 mM L-glutamine, 1 × nonessential amino acids, 100 mM β-mercaptoethanol), supplemented with 4 ng/ml of basic fibroblast growth factor (all reagents from Thermo Fisher). Cells were manually passaged weekly. Single iPSC colonies were cut using a syringe needle and the pieces transferred to new feeder coated wells.

2.5. Karyotyping and a-CGH of iPSC clones

The cytogenetic analysis was performed using QFQ-banding techniques on metaphase chromosomes obtained by standard procedures from peripheral blood lymphocytes and from iPSC clones at passages from P4 to P8. At least 30 metaphases were scored in each case.

Genomic blood DNA was extracted by the means of GenElute Blood Genomic DNA kit (Sigma-Aldrich, St. Louis, MO, USA); iPSC genomic DNA was extracted from iPSC clones (P4-P8) by Wizard Genomic DNA Purification Kit (Promega, Madison, WI, USA).

High-resolution array comparative genomic hybridisation (array-CGH) was performed on genomic blood and iPSC DNA using the SurePrint G3 Human CGH Microarray Kit 2x400K and 4x180K in accordance with the manufacturer's instructions (Agilent Technologies, Palo Alto, CA,USA). Probe positions are referred to human genome assembly GRCh37/hg19.

2.6. Characterization of genetic defects in iPSC cell lines

Genomic DNAs from iPSC clones controlled for genomic stability were subjected to bi-directional Sanger sequencing (Applied Biosystems, Carlsbad, CA, USA) to disclose the original *CREBBP* or *EP300* mutation, as described (Bentivegna et al., 2006; Spena et al., 2015; Negri et al., 2016).

Transcript analysis was performed using the primers previously employed on lymphoblastoid cell line/peripheral blood from *CREBBP*-mutated patient #46 (Lopez-Atalaya et al., 2012) and *EP300*-mutated patients #65 and #207 (Negri et al., 2016). New primers pairs were designed for *CREBBP*-mutated patients #149 (c.*CREBBP*_Ex17F 5′-TACGCCAGGCCCTCATG-3′/c.*CREBBP*_Ex19-20R 5′-CAGAAATGATA CCTATTCTG-3′) and #158, (c.*CREBBP*_Ex26F 5′-TACCATGAGATCCTT ATTGGAT-3′/c.*CREBBP*_Ex29-30R 5′-AGAAGACCTCCTTGTGCT-3′), while the primer pair designed for #46, was also used to detect transcripts of patient #34 iPSCs.

2.7. Western blot

iPS cell extracts (120 μg) were separated on NuPAGE 4–12% Bis-Tris Gel (Invitrogen, Waltham, MA, USA), transferred to nitrocellulose and blocked with 5% BSA in PBS-0.2% Tween 20 (PBS-T). The membrane was incubated for 1 h at RT with rabbit polyclonal anti CBP (A-22) (sc-369)1:300 or rabbit polyclonal anti p300 (N-15) (sc-584) 1:300 (both Santa Cruz, Dallas, TX, USA) and anti-actin mouse monoclonal 1:2.000 (Sigma-Aldrich, St Louis, MO, USA) followed by washings in PBS-T and

Table 1
Patients selected for iPSCs: age, affected locus, type of mutation and predicted effect on protein, neuropsychological assessment at reprogramming, main clinical features and references on previous clinical and molecular characterization.

Patient code sex age (y)	Gene	Mutation site and predicted effect on protein	RSTS dysmorphisms	Growth retardation	Neuropsychiatric Assessment		Skeletal anomalies		Organ malformation	Cancer development	References
					IQ*/GQ°	Behavioural profile #	Broad thumbs	Broad halluces			
CREBBP NM_004380											
34 M (12)	Exon 27	c.4435G > T p.(Gly1479*)	+	+	47*	Normal	+	−	−	−	Bentivegna et al., 2006
46 F (13)	Exon 28	c.4627G > T p.(Asp1543Tyr)	+	+	61*	Behavior disorder	+	+	Renal hypoplasia	Multiple pilomatricoma	Bentivegna et al., 2006 Lopez-Atalaya et al., 2012
149 M (6)	Exon 18	c.3474G > A p.(Trp1158*)	+	+	25°	ASD	+	−	Cerebellar hypoplasia, corpus callosum agenesis, cryptorchism, feet polidactyly	−	Spena et al., 2015
158 F (5)	Exon 28	c.4650-4654del p.(Glu1551Hisfs*2)	+	+	45°	Normal	+	−	PDA, pulmonary valve stenosis	Hepatoblastoma	Spena et al., 2015 Milani, 2016
EP300 NM_001429											
65 M (25)	Exon 23	c.3829A > T p.(Lys1277*)	+	+	"Mild"	ADHD	+	+	−	Multiple naevi	Negri et al., 2016
207 M (19)	IVS 9	c.1878-12A > G p.(Ala627Glnfs*11)	+	+	42*	behavior disorder	+	+	−	−	Negri et al., 2016

*Assessed by Leiter R (*) or Griffith's scale (°), assessed by CBCL, SCQ (#).

incubation for 30 min at RT in HRP-labeled secondary anti-rabbit and anti-mouse antibodies 1: 2.000 (Thermo Fisher Scientific). Chemiluminescence signals were revealed with a Westar R imager (Hi-Tech Cyanagen, Bologna, Italy).

2.8. In vitro differentiation of iPSCs to cortical neurons

Clones which bypassed the check for genome stability were differentiated into cortical neurons according to the monolayer protocol in N2B27 medium (Neurobasal medium, 2% B27, 1% Insulin Transferrin Selenium, 1% N2, 2 mM L-Glutammine, 0.5% P/S) (all reagents from Thermo Fisher Scientific, Waltham, MA, USA) supplemented with 500 ng/ml Noggin (R&D Systems, Minneapolis, MN, USA) (Germain et al., 2014). Once, usually after 14–16 days, neural rosettes appeared, they were manually passaged on poly ornithine-laminin (Sigma-Aldrich, St Louis, MO USA) coated dishes and maintained in the same medium for further two weeks. At day 28 the N2B27 medium was changed to Neural Differentiation Medium (Neurobasal medium, 2% B27, 1% NEAA, 2 mM L-Glutammine) (all reagents from Thermo Fisher), plus 10 ng/ml BDNF, 10 ng/ml GDNF (both from Peprotech, London, UK), 1 μM Ascorbic Acid and 200 μM cAMP (both from Sigma-Aldrich). After one week neural progenitor cells (NPCs) were plated at low density (1×10^5–1.5×10^5 cells in a 9.6 cm^2 well) for terminal differentiation and not passaged any more. NPCs could be frozen and thawed without loss of potency. Neurons were maintained in culture by half media changes twice a week until 70 or 100 days.

2.9. Immunofluorescence staining

Cells were fixed in 4% paraformaldehyde for 20 min at 37 °C. Primary antibodies were applied at 4 °C overnight. Secondary antibodies were incubated with cells for 2 h at room temperature. The following antibodies were used: Oct3/4 (sc-9081)1:200, Tra-1-60 (sc-21705) 1:100, CUX-1 (sc-13,024) 1:100 (Santa Cruz Biotechnology, Dallas, TX, USA); Nestin (ab22035) 1:300, Map2 (ab32454) 1:300, TBR1 (ab31940)1:200, Synaptophysin (ab14692) 1:200 (Abcam, Cambridge, UK); TUJ1 (801201) 1:500, Pax6 (PRB-278P) 1:300 (Covance Princeton, NJ, USA); Anti-GAD 65/67 (AB1511) 1:100; Anti V-GLUT1 (MAB5502) 1:100 (Millipore Burlington, MA, USA); Goat anti mouse Alexa fluor 488 (1:500), Goat anti rabbit Alexa fluor 555 (1:300) (Thermo Fisher). DAPI was used to counterstain cell nuclei. Bright field images were acquired with JuLITM cell analyzer (10–20× digital zoom). Confocal images of 1024 × 1024 pixels were obtained with Nikon Eclipse Ti microscope.

2.10. RT-PCR

Total RNA was isolated from iPSCs using Trizol reagent and 1 μg was retro-transcribed using SuperScript Vilo (Thermo Fisher) according to manufacturer's instructions. cDNAs were amplified using GoTaq (Promega, Madison, WI, USA).The following primers (designed by Dr. V. Silani's group, Milano) were used to amplify Nanog: forward CAGC CCTGATTCTTCCACCAGTCC and reverse GTTCTGGAACCAGGTCTTCA CCTG. The amplification of *OCT3/4* and *SOX2* genes was performed using primers reported by the Yamanaka's group (Takahashi et al., 2007).

2.11. Morphological characterization of neural progenitors

Morphological analysis of branches (average branch length and average branch number) was performed on 42–day-old neurons stained for TUJ1. All 1024 × 1024 pixels images were acquired with Nikon Eclipse Ti confocal microscope and 40× objective. 30–50 cells were selected for every sample and analyzed by the ImageJ plugin Analyze Skeleton (Arganda-Carreras et al., 2010).

2.12. Electrophysiology recordings of differentiated neurons

Whole-cell patch-clamp recordings were performed on 70-day-old differentiated neurons at room temperature (~25 °C) using a

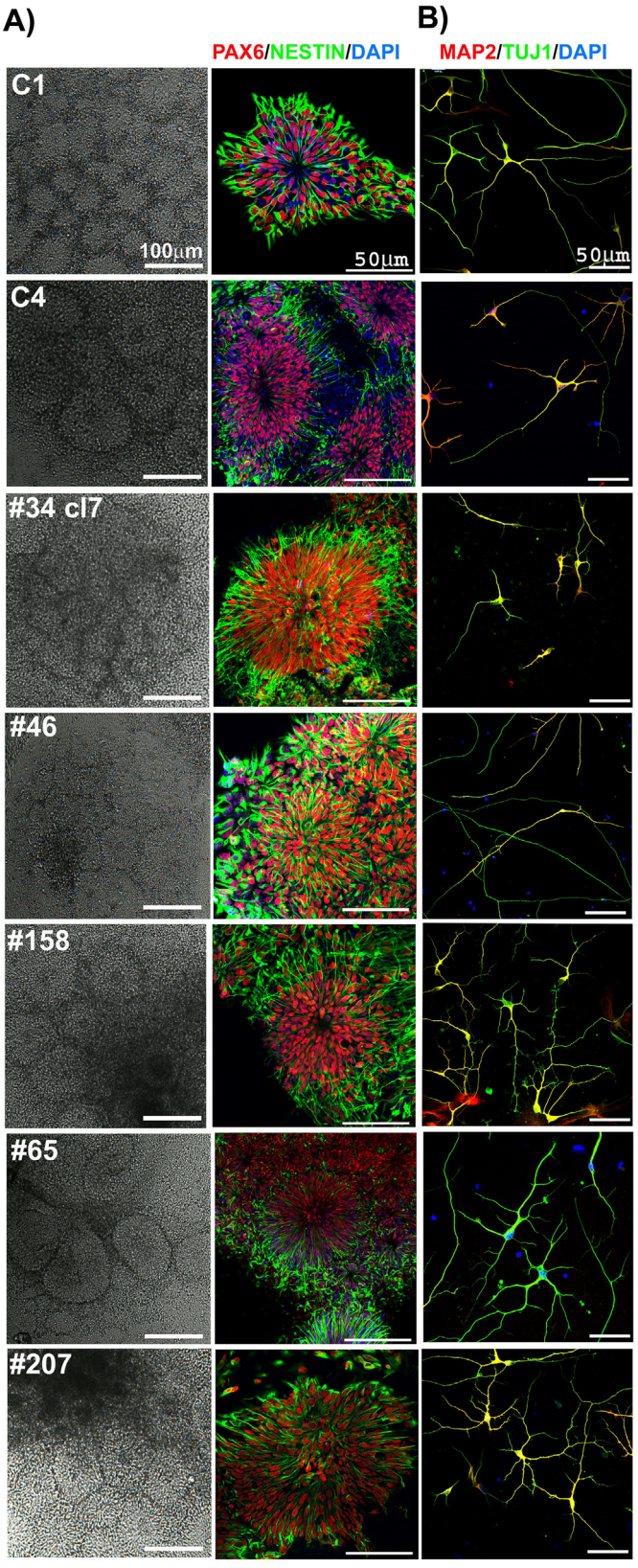

Fig. 1. Immunofluorescence and morphological characterization of iPSC-derived neural progenitors and early neurons. A) Left: bright-field images of neural rosettes (10×) from C1, C4, #34cl7, #46, #158, #65 and #207. Right: immunofluorescence positive staining of the neuroectodermal stem cell markers NESTIN and PAX6 on coverslips from C1, C2, #34cl7, #46, #158, #65 and #207. Scale bar 50 μm. B) Immunostaining of 42-day-old neurons from the same controls and patients showing positivity for the pan neuronal cell markers MAP2 and TUJ1. Nuclei are counterstained with DAPI. Scale Bar 50 μm.

Multiclamp 700A amplifier and pClamp 10.5 software (Molecular Devices, Sunnyvale, CA, USA) in voltage- or current-clamp configuration, as in Verpelli et al., 2013 and Terragni et al., 2016. Signals were filtered at 10 kHz and sampled at 200 kHz for voltage-clamp recordings or 20 kHz for current-clamp recordings. External bath solution contained (mM): 129 NaCl, 1.25 NaH_2PO_4, 35 glucose, 1.8 $MgSO_4$, 1.6 $CaCl_2$, 3 KCl and 10 HEPES, pH 7.4 with NaOH. The internal pipette solution contained (mM): 120 K-gluconate, 15 KCl, 2 $MgCl_2$, 0.2 EGTA, 10 HEPES, 20 phosphocreatine-tris, 2 ATP-Na_2, 0.2 mM GTP-Na_2 and 0.1 leupeptin, pH 7.2 with KOH. Pipette resistance was between 3 and 4 MΩ. Cell capacitance and series resistance errors were carefully compensated (~85%) throughout the experiment. The remaining linear capacity and leakage currents were eliminated online using a P/4 subtraction paradigm. Total voltage-gated currents were elicited by applying 66 ms-long depolarizing voltage steps from −70 to +60 mV (10 mV increments), from a holding potential of −70 mV. Sodium and potassium current densities were obtained by dividing the recorded currents for the cell capacitance, measured by integrating the capacitative current evoked by a 10 mV hyperpolarizing voltage step from the holding potential. Discharges of action potentials (APs) were evoked by the injection of 2.5 s-long depolarizing current pulses of increasing amplitude from the resting potential maintained at −70 mV. The input-output relationship is the plot of the number of APs generated vs. the amplitude of the injected current. Rheobase was defined as the minimal current amplitude needed to reach the threshold for action potentials. AP threshold was calculated with the first derivative method.

2.13. Statistical analyses

Morphological characterization: differences in number and average length of neural progenitors branches were evaluated by a Kruskal-Wallis test followed by Dunn's Multiple comparison test with Bonferroni's correction. Correlation analysis of these two features was performed by using Spearman's rank correlation. Analyses were conducted in R environment by using specific packages. Graphics (box-plots and scatter-plots) were generated through GraphPad Prism (V.7) software.

For electrophysiological experiments, graphics and statistical analysis were obtained using pClamp and Origin 8 software. Proportions (percentages of neurons with sodium current or generation of APs) were analyzed with Fisher's exact test. Data on sodium and potassium current densities, input-output relationship, membrane capacitance, rheobase and AP threshold are given as mean ± SEM and were analyzed with ANOVA and Bonferroni post-test.

Statistical significance was set at $p = 0.05$

The workflow of iPSC generation and characterization is outlined in Suppl. Fig. 1.

3. Results

3.1. Neuropsychiatric assessment of RSTS- patients selected for iPSC generation

"Ad hoc" neuropsychiatric assessment, including Intellectual Quotient (IQ) or General Quotient of Development (GQ) according to patient age and behavioural characteristics was performed by the same neuropsychiatrist (P.F.A.) in parallel to iPSCs generation (patients #34, #46, #149 and #207). Updated evaluation was obtained by contact with the local neuropsychiatrist for patients #65 and #158. Table 1 provides for the six patients the age at withdrawal for iPSC generation, the affected *CREBBP* or *EP300* locus, the location and type of pathogenic variant and predicted effect on the protein, the assessed score of intellectual level plus the presence/absence of behaviour disorder and the main RSTS clinical features. These are detailed together with the molecular characterization in the attached references. Out of the four *CREBBP*-mutated patients, a mild ID (intellectual disability according to

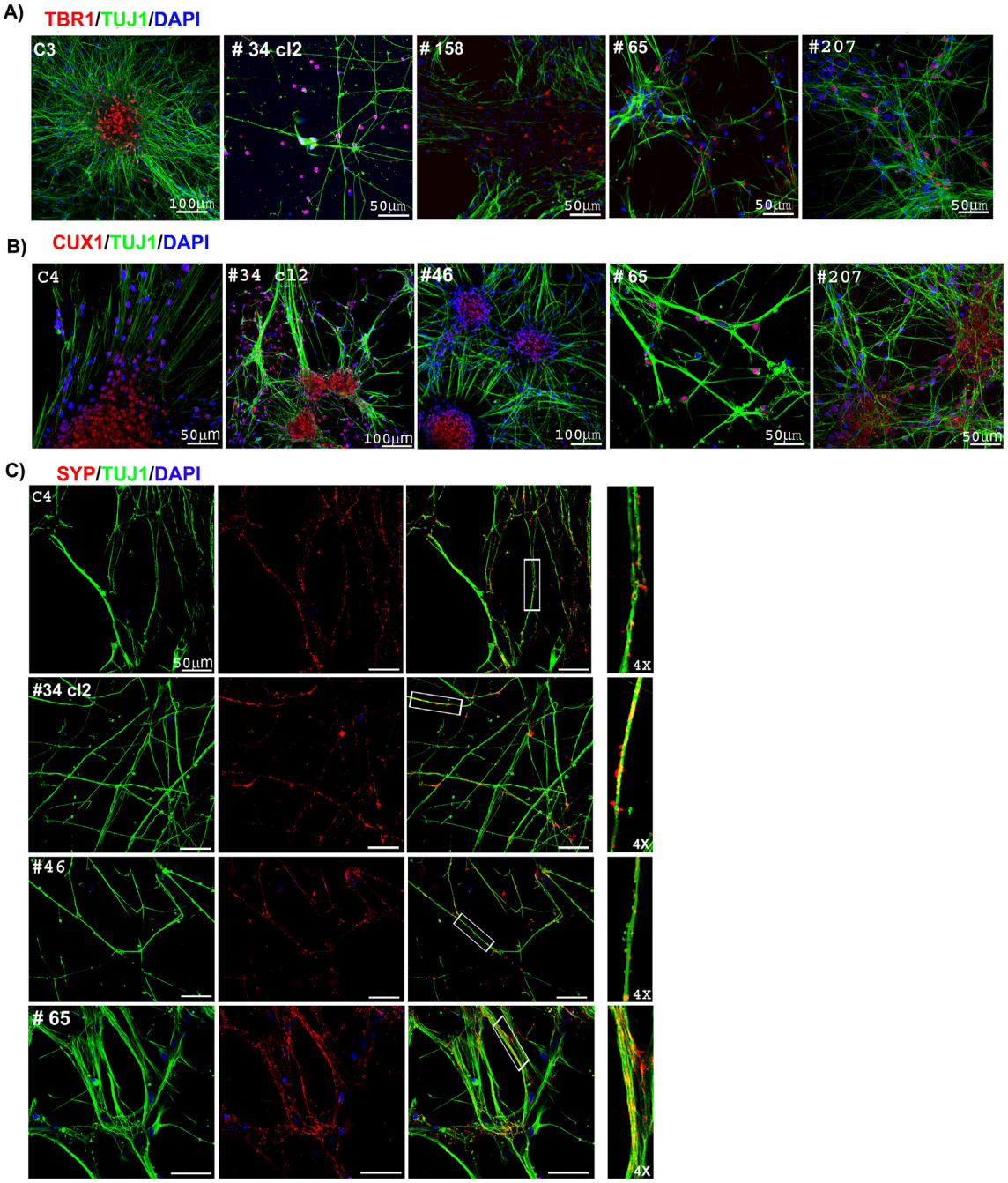

Fig. 2. Immunofluorescence characterization of cortical markers in patient-specific 70 days i-neurons. A) Positive immunostaining of TUJ1 and the early cortical marker TBR-1 in C3, #34cl2, #158, #65 and #207 neurons. B) Representative pictures of C4, *CREBBP*-mutated #34cl2, #46 and *EP300*-mutated #65 and #207 neurons showing the positive immunostaining of TUJ1 and the post-mitotic cortical neurons marker CUX-1. C) Positive immunostaining of synaptophisyn (SYP) and TUJ1 in neurons from C4, 34cl2, #46 and #65. The insets show a 4× magnification view of framed fields of merge images of immunolabeled cells.

ICD 10 classification) is assigned to #46 carrying a missense mutation in the KAT domain, while patients #149, #34 and #158 carrying inactivating mutations predicted to lead either to haploinsufficiency or to truncated proteins lacking all or part of KAT and downstream domains, have in the order a severe or moderate ID according to IQ/GQ scores. Based on parents' point of view clinical scores of ASD are present in patient #149 who is placed at the most severe end of the ID spectrum of this RSTS cohort. Behavioural disorder is not observed for patients #34 and #158, while high social anxiety, difficulties in peer-relationship and withdrawn behaviours are recorded for the best performing *CREBBP*-mutated patient #46.

As to the two adult *EP300*-mutated patients, #65 carrying a non sense mutation predicting a protein, if any, lacking the KAT and downstream domains, has definitely a mild ID (he achieved a diploma in social sciences) and only suffered from attention deficit hyperactivity disorder, while #207 carrying an IVS9 variant yielding a cryptic acceptor splice site and out-of-frame transcript predicting early protein truncation combines a moderate ID with a severe behavioural disorder (Negri et al., 2016).

3.2. Generation and characterization of RSTS-specific iPSCs

iPSCs were generated from PBMCs of the above listed RSTS patients and four control subjects using the Sendai virus (SeV) non integrative

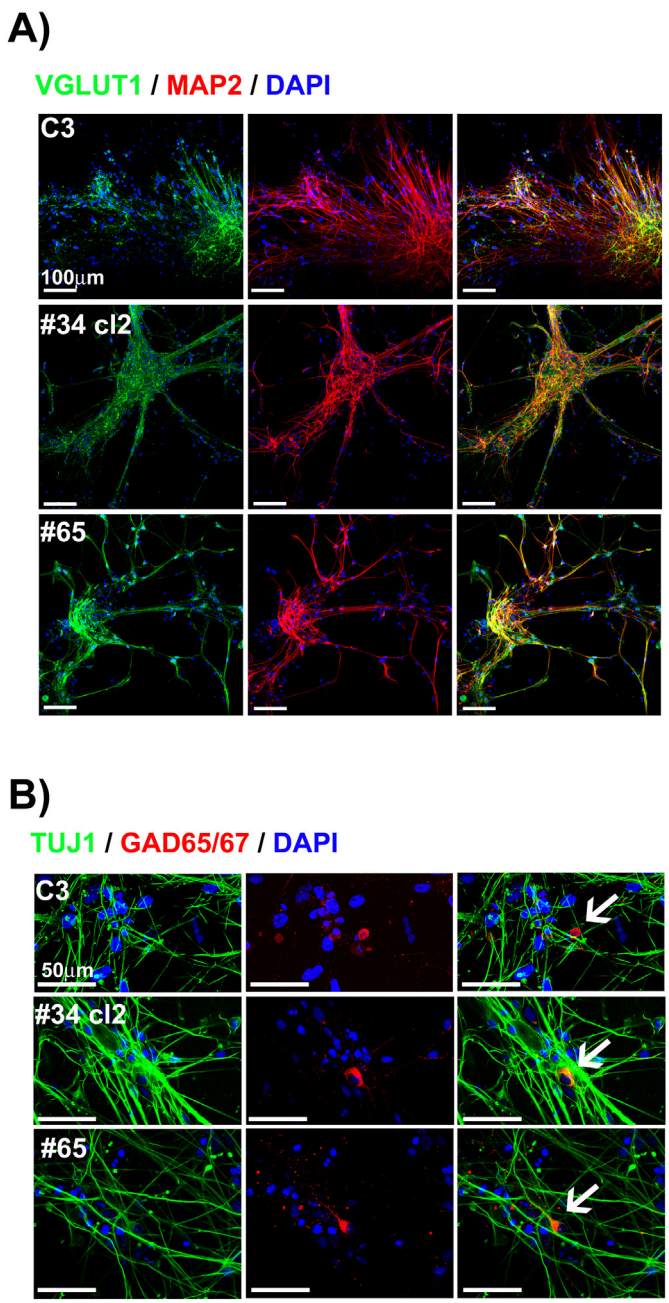

Fig. 3. Immunofluorescence characterization of excitatory and inhibitory markers in patient-specific 70 days i-neurons. A) Positive immunostaining of the glutamatergic subtype-specific marker vesicular neurotransmitter transporter 1/2 (vGLUT1/2) and MAP2 in neurons from C3, *CREBBP*-mutated #34cl2 and *EP300*-mutated #65. Scale bar 100 μm. B) Immunostaining of TUJ1 and the inhibitory subtype-specific marker glutamic acid decarboxylase 65/67 (GAD65/67) in neurons from the same samples shown in A). The white arrows point to the rare GAD65/67 stained neurons. Scale bar 50 μm.

reprogramming method which is currently mostly used for its efficiency, safety and simple handling (Soares et al., 2016). Two controls, C2 and C3, mother and brother of patients #149 and #34, respectively, fulfil the family design, allowing the genetic background to be controlled in future application of the in vitro model. For each individual three iPSC clones were characterized by karyotyping and array CGH and genomic DNAs of clones without any cytogenetic or submicroscopic rearrangement were checked for the presence of the original mutation by Sanger sequencing. As exemplified in Suppl. Fig. 2 clone 3 from patient #34 maintained the normal 46,XY karyotype (Suppl. Fig. 2A), but its genomic DNA evidenced by array-CGH a rare Copy Number Variant (CNV) at chromosome 3p14.3 (Suppl. Fig. 2B) not present in the peripheral blood, letting to discard this clone. Clones 2 and 7 were then checked for the presence of the original c.4435G > T pathogenic variant (Suppl. Fig. 2C) and characterized for iPSC markers by immunofluorescence microscopy and RT-PCR.

We scored an overall frequency of 24% rearranged iPSC clones, but a frequency of 7% would have been detected by karyotyping alone.

Characterization of the iPSC clones included transcript and western blot (WB) analyses. Aberrant transcripts were observed in all *CREBBP*- and *EP300*-mutated iPSC lines though their fluorescence peaks appeared less represented than those encoded by the wild-type allele, with the only exception of patient #46, carrier of a *CREBBP* missense mutation, which aberrant transcripts were comparable to the wild-type ones (Suppl. Fig. 3). Accordingly, Western blot analysis using antibodies directed against the N-terminal portion of CBP/p300 evidenced the expression of a full-length protein, corresponding to the wild-type protein in reduced amount in the iPSC lines from patients with inactivating gene mutations and in the same amount of control in #46 iPSC line (data not shown).

Valid iPSC clones entered the characterization for the pluripotency markers Oct3/4, TRA-1-60 and Nanog by immunofluorescence (IF) and Oct3/4, SOX2 and Nanog by RT-PCR. We confirmed that iPS clones from all six RSTS patients and four controls expressed the human pluripotency-associated gene products. Suppl. Fig. 4A shows the bright-field image of an iPSC colony of C1, C3, of the four *CREBBP*-mutated #34, #46, #149 and #158 and of the two *EP300*-mutated #65 and #207 patients and the positive expression at confocal microscopy of Oct3/4 and TRA-1-60 in all the immunostained samples. Parallel characterization involved RT-PCR expression analysis of Oct3/4, Sox2 and Nanog, as can be seen for four iPS clones from C1 and from #34 and #207 patients (Suppl. Fig. 4B).

3.3. From iPS colonies to neurons

Application of the monolayer protocol in N2B27 medium supplemented with noggin (Germain et al., 2014) induced iPS colonies from all four controls and five RSTS patients to start and complete neuronal differentiation. Two iPSC lines could be differentiated from patients #34, #46, #158 and #207.

Neural differentiation is first marked by the appearance of the typical neural rosettes (day 20) which by manual cut and culture passaging are further induced to differentiate into neural progenitors (NPCs) (day 35). At the rosette stage the majority of cells from control and RSTS-iPSCs showed positive IF staining for the neuroectodermal stem cell markers NESTIN and PAX6 (Fig. 1A). Foxg1, a member of the forkhead-box family of transcription factors and Sox1, a member of the SoxB1 family of transcriptional activators, both among the earliest markers of neural stem cell identity, were also expressed in rosettes from patients and controls (data not shown). NPCs self-renewed, maintained their differentiation potential and were further induced to differentiate into neurons. We confirmed by IF that 42-day-old neurons from both controls and all five RSTS patients expressed the neuronal markers MAP2 (microtubule-associated protein 2) and TUJ1 (betaIII-tubulin). Representative images are shown in Fig. 1B. We made use of this stage at which neurons are at low density in culture to assess on immunostained coverslips whether the morphological characteristics of neurons differed between controls and patients (see Section 3.4.)

After prolonged maintenance in culture (70 days) both control and patient i-neurons developed a highly intricate network of cells enriched in cortical neurons, as shown by expression of the T-Brain-1 (TBR-1) transcription factor, a master regulator of cortical development, the cut-like CUX-1 homeodomain transcription factor, necessary for dendrite development of cortical neurons, and the presynaptic marker synaptophisyn (SYP). Representative images of TBR-1, CUX-1 and SYP-stained coverslips from controls, *CREBBP*- and *EP300*-mutated patients are

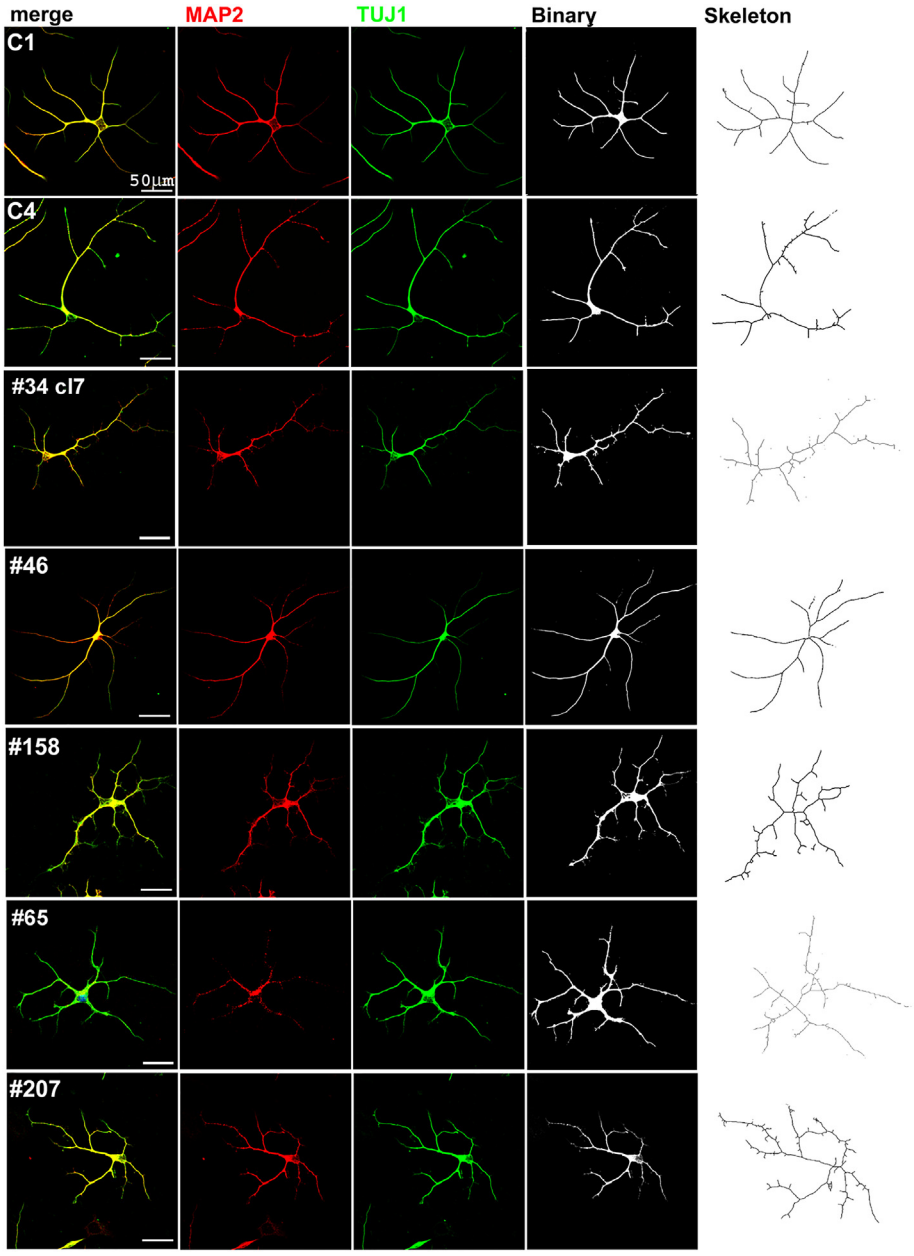

Fig. 4. Morphological analysis of 42 days neurons from patient-specific iPSCs. Positive immunostaining of MAP2 and TUJ1 confirms the neuronal identity of the differentiating single cell of C1, C4, #34cl2, #46, #158, #65 and #207. Nuclei are counterstained with DAPI. Scale Bar 50 µm. The right panels show the binary and the skeletonized images.

shown in Fig. 2A–C. Both in control and patient cultures CUX-1 positive cells were mostly concentrated in the dense clusters, and were few or absent in culture areas close to mound or sparse (Fig. 2B). Most i-neurons from control, *CREBBP*- and *EP300*-mutated patients were also positive for the glutamatergic subtype-specific marker vesicular neurotransmitter transporter 1/2(vGLUT1/2), while few were positive for the glutamic-acid decarboxylase 65/67 (GAD65/67) inhibitory marker (Fig. 3A–B)

3.4. Morphological analysis of 42 days neurons from RSTS and controls

Due to its 2D nature, the monolayer neuronal differentiation system used enabled us to analyze cellular morphology, such as neurite length and average number of branches on coverslips from 42-day-old neurons from control and RSTS patients by the Plugin “Analyze Skeleton” (Image J) (Arganda-Carreras et al., 2010).

As shown in Fig. 4 the same single cell confirmed by positive immunostaining of MAP2 and TUJ1 to be a neuron, is elaborated as binary image and skeletonized allowing the neurons branch length and average number to be precisely counted. Analysis of an average of 30–50 cells from each sample, including controls (C1, C3, C4) and five RSTS patients, three *CREBBP*-mutated (#34-cl 7 and cl 2-, #46 and #158) and two *EP300*-mutated (#65 and #207) allowed to graph these measures. Scores for C1, C3 and C4 were pooled together as well as those from the two independently differentiated iPS lines from #34 as the slight inter-culture variability was not significant (data not shown).

The box-plots in Fig. 5A show that neurons from RSTS patients #34, #207, #65 and #158 have an average branch length significantly reduced as compared to that of controls while the values of patient #46 neurons cluster with those of controls. The box-plots in Fig. 5B evidence a similar opposite trend for variations in the average branch number with neurons from #46 similar to controls and those from the other

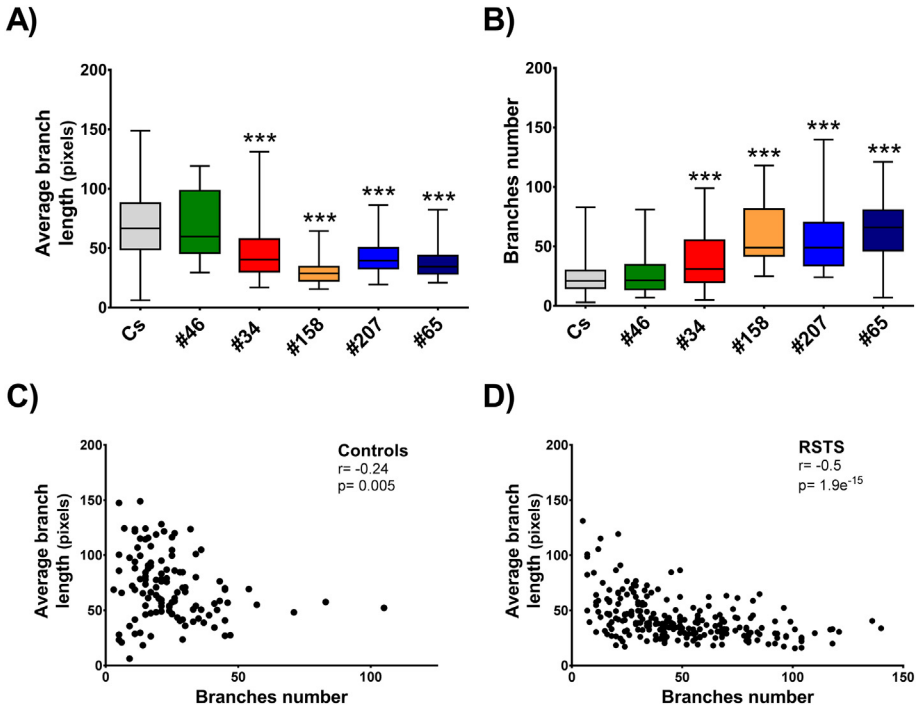

Fig. 5. Statistical analyses of morphological features obtained from 42 days neurons of patient-specific iPSCs. A–B) Box-plots showing the average length (A) and number (B) distribution of neuronal branches from pooled controls (Cs) and RSTS #46, #34 (clones 2–7 pooled) #158, #207 and #65 patients. Data are shown as median and interquartile range; whiskers represent maximum and minimum values. Data were acquired by using the "Analyze Skeleton" plugin (Image J) (***$p < 0.001$). C–D) Scatter plots showing the average length of neuronal branches as function of branch number in controls (C) (121 cells) and RSTS patients (D) (235 cells). Correlation coefficients (r) and p-values (p) are also shown.

patients displaying an arborisation increasing from #34, #207 and #158 to #65, significantly higher than controls. The opposite trend in neurons of RSTS patients is confirmed by correlation analysis of these two features (Fig. 5C-D): the average length and number of neuronal branches are negatively correlated ($r = -0.5$, p = 1.9e−15, CI 95%: −0.582 to −0.380) while the correlation in controls cells appear to be consistently lower or weak ($r = -0.24$, p = 0.005, CI 95%: −0.414 to −0.069).

3.5. Electrophysiology of mature cortical neurons

Neurons obtained from control (C4), *CREBBP*- #34, #46 and *EP300*-mutated patients #65 and #207 were analyzed by patch-clamp recordings after 70 days of differentiation to test their maturity and characterize their cellular excitability. Voltage-clamp experiments showed the expression of voltage-gated sodium and potassium currents, similarly to mature neurons, as shown by the representative current traces in Fig. 6A (top panels). A more detailed analysis revealed that the majority of neurons, from both control and patients, expressed voltage-gated sodium currents with comparable peak amplitudes (C4: −141.4 ± 13.8 pA/pF, $n = 25$; #34: −180.3 ± 17.7 pA/pF, $n = 28$; #46: −131.1 ± 22.7 pA/pF, $n = 13$; #207: −122.6 ± 23.3 pA/pF, $n = 16$; #65: −151.7 ± 20.9 pA/pF, $n = 18$; ANOVA and Bonferroni post-test, $p > 0.05$). Voltage-gated potassium currents had similar amplitude in neurons from control and patients #46, #207 and #65, while in neurons from patient #34 they were slightly but significantly increased at −10, 0, +10 and +20 mV with respect to control currents (C4: 7.9 ± 1 pA/pF, 16.7 ± 1.9 pA/pF, 34.5 ± 3.6 pA/pF, 56.1 ± 5.9 pA/pF at −10, 0, +10, +20 mV, respectively, n = 25; #34: 23.2.7 ± 2.6 pA/pF, 38.7 ± 3.9 pA/pF, 59.3 ± 5.2 pA/pF, 82 ± 7 pA/pF at −10, 0, +10, +20 mV, respectively, n = 28; ANOVA and Bonferroni post-test, ($p = 5.1 \times 10^{-8}$ at −10 mV, $p = 5.3 \times 10^{-7}$ at 0 mV, $p = 1.1 \times 10^{-4}$ at +10 mV, $p = 9.7 \times 10^{-3}$ at +20 mV) (Fig. 6A, bottom panels). Current-clamp experiments confirmed the maturity of differentiated neurons, because they were able to generate discharges of action potentials in response to depolarizing stimuli (Fig. 6B, top panels). Interestingly, a lower percentage of neurons from patients #34 and #207 produced action potentials with respect to control ones (Fisher's exact test, p = 0.007 for pt. #34, p = 0.038 for pt. #207); moreover, neurons from all the investigated patients were less excitable, as shown by the input-output relationships (ANOVA and Bonferroni post-test) (Fig. 6B, bottom left and middle panels). To test whether the observed diminished efficiency of patients' neurons in generating action potentials correlated with modifications in cell capacitance, rheobase and/or AP threshold, we quantified and compared these parameters between patients and control and disclosed an increased rheobase for neurons from patients #46 ($p = 7.7 \times 10^{-5}$) and #207 ($p = 1.8 \times 10^{-2}$) together with a depolarized AP threshold for neurons from patient #207 ($p = 1.8 \times 10^{-2}$), thus indicating the requirement of higher stimulus intensities to reach the threshold for generating APs (ANOVA and Bonferroni post-test) (Fig. 6B, bottom right panel). Neurons from patient #34 did not show modifications of these parameters, therefore their hypoexcitability may be caused by additional mechanisms.

4. Discussion

We established the first in vitro iPSC-derived neuronal model for RSTS which "per se" demonstrates that the deficit of CBP/p300 resulting from *CREBBP/EP300* haploinsufficiency or defective protein function does not interfere with reprogramming and pluripotency and does not preclude the capability of iPSC-derivatives to progress till neurons.

As regards the first step of the model, we could successfully reprogram to iPSCs blood cells from all the six selected RSTS patients and from the four controls and carefully checked for maintenance of genomic stability at least three iPSC clones per donor. The frequency of rearranged iPS clones we recorded raised from 7% by karyotyping to 24% by high-resolution array-CGH. A study on comparison of non integrating reprogramming methods showed for iPSC generated by SeV an aneuploidy rate of 4.6% by karyotyping, whereas the frequency of CNVs by small-scale genome-wide array aCGH was said to be uniformly low (Schlaeger et al., 2015). It is worth noting that the rate of detection of acquired CNVs depends on the array resolution, accounting for the high frequency of CNVs detected by our high-resolution (180-400 K) array platform. Non random CNVs, often conferring to the carrier cells proliferative advantage in vitro may be found in iPSC lines with normal karyotype as shown by the chromosome 20q11.21 gain identified by

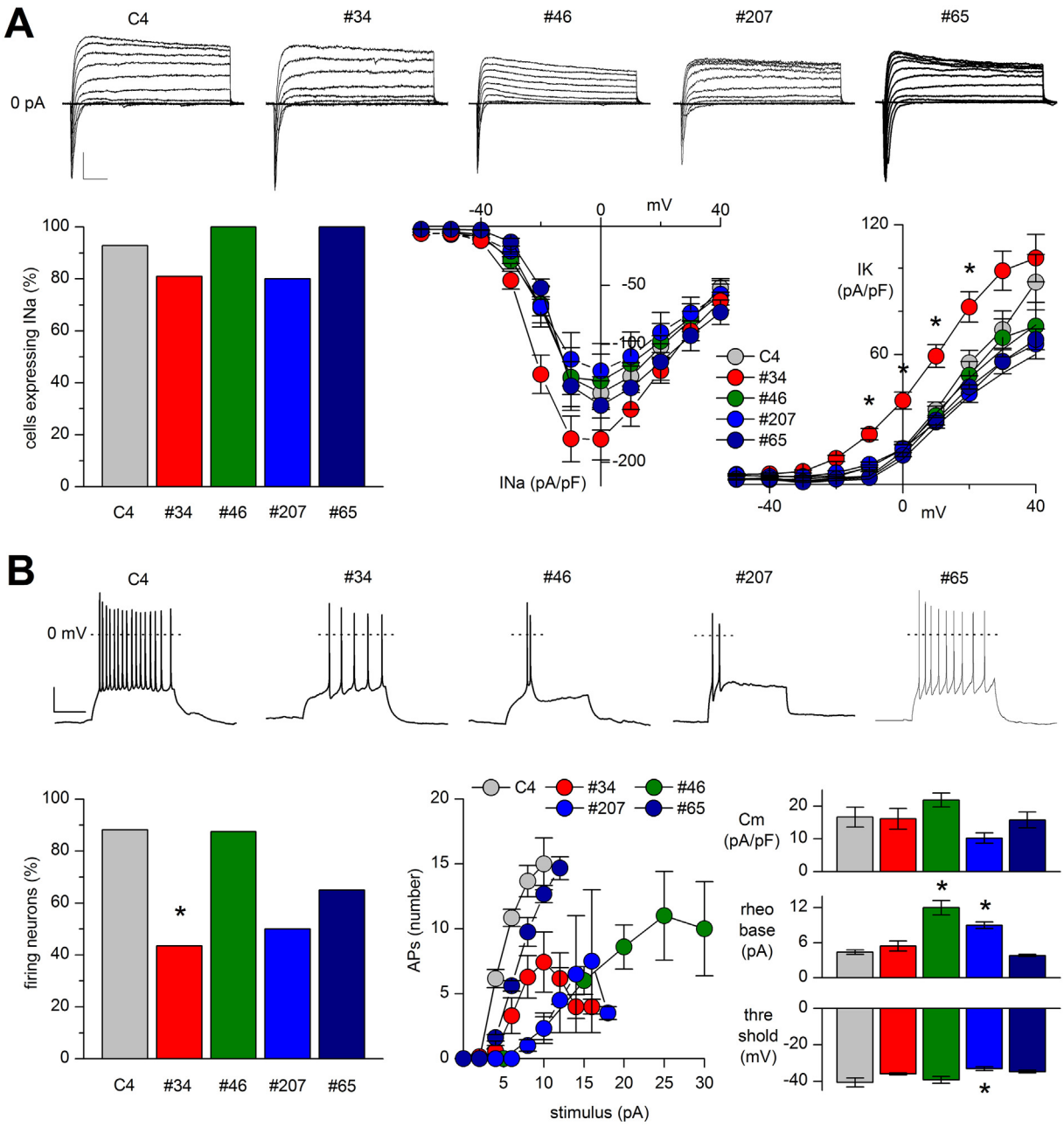

Fig. 6. Electrophysiological characterization of neurons from control and patients after 70 days of differentiation. A) Top panels: representative total ionic currents elicited with depolarizing voltage steps between −70 and +60 mV, from a holding potential of −70 mV (scale bars: 50 pA/pF, 10 ms). Bottom panels: quantification of % of neurons with sodium current (left), sodium (middle) and potassium (right) current densities at different potentials. Potassium current density was increased in neurons from patient #34, which also showed a trend for increase of sodium current density. B) Top panels: representative discharges of action potentials (APs) evoked by the injection of 2.5 s-long depolarizing stimuli at the intensity of 8–10 pA (scale bars: 20 mV, 1 s). Bottom panels: quantification of % of neurons able to generate APs (left) and input-output relationships (middle). With respect to control neurons, a decreased percentage of neurons from patients #34 and #207 generated APs. Neurons differentiated from patients generated less APs in input-output relationships than neurons differentiated from control (statistically significant differences are not indicated in the graph for clarity, see text). Quantification of cell capacitance (Cm), rheobase and AP threshold (right); rheobase was increased in neurons from patients #46 and #207, AP threshold was depolarized in neurons from patient #207.

the "International Stem Cell initiative" (Amps et al., 2011) in > 20% of human embryonic and iPSC stem lines. Our data recommend appropriate check of genome stability, both for correct evaluation of the cellular phenotype of the patient iPSC-derived neurons and perspective medical applications.

We confirmed the patient-specific pathogenic variants in *CREBBP* and *EP300* in the iPSC lines by Sanger sequencing. Aberrant transcripts were observed in iPSCs from all patients, though, with the exception of #46, are featured by the respective fluorescence peaks as residual transcripts escaping non sense mediated decay. Consistent with this data, western blot analysis did not reveal in the RSTS iPSC lines truncated proteins, but haploinsufficiency-dependent reduction in the wild-type CBP/p300 protein, except patient #46 showing the same quantity of full length CBP protein of control iPSC line (data not shown).

We could obtain iPSC-neuronal cultures from all controls and three out of four *CREBBP*- and two out of two *EP300*-mutated patients. The fourth *CREBBP*-mutated patient #149 has currently progressed till the stage of neural progenitors.

Consistent with the protocol employed to induce differentiation of iPSCs to cortical neurons, pan neuronal (TUJ1, MAP2) and cortical-

specific markers (TBR-1 and CUX-1) were expressed by all patients' neurons. It is known from mice models that Cbp regulates neural cell genesis and cortical precursor differentiation and Cbp haploinsufficiency or genetic knockdown causes a small but significant decrease in the number of neurons generated, leaving intact proliferation and survival (Valor et al., 2011; Wang et al., 2010).

As a quantitative study to define the percentage of TUJ1-positive cortical precursors and CUX-1 glutamatergic neurons, which are abundant in RSTS i-neurons, could not be pursued on the numerous RSTS and control iPSC-derivatives, based on the knowledge that morphological maturation precedes functional maturation in a iPSC-derived neuronal differentiation model (Kang et al., 2017) we evaluated morphological analysis of differentiating neurons (42-days) and electrophysiological profiles of differentiated neurons (> 70 days) to disclose potential structural and functional differences between control and patient-specific neuronal cultures.

We monitored significant reduction in branch length and increase in branch number with respect to control in differentiating neurons of four out of five analyzed patients. The observed increase in branches number is not consistent with the reported reduction in dendritic protrusions of iPSC-neurons from other neurodevelopmental disorders (Nagy et al., 2017; Kim et al., 2014; Linda et al., 2018). This discrepancy may be accounted by the earlier timing of our analysis, which implies possible spine abortion and hence decreased number in terminally differentiated neurons. That the observed morphological alterations are patient-specific is pointed out by the similar ranking in neurons of each patient of both evaluated parameters. As to the clustering with controls of #46, it may reflect a genotype-related difference as she is the only patient carrying a missense mutation causing a defective KAT activity not leading to haploinsufficiency. A limited effect of mutant Cbp proteins carrying missense mutations in the KAT domain, including mutations associated to RSTS, has been demonstrated on primary embryonic fibroblasts from Cbp/p300 cre-deleted double knock-out mice that retain significant KAT activity, as acetylation of a known histone substrate was attenuated, but not blocked and differed between mutants (Mullighan et al., 2011). One may speculate that the mutant CBP protein might cause impairment at a later stage of neuronal differentiation, as inferred by the electrophysiological recordings of #46's fully differentiated i-neurons.

Importantly, the electrophysiological studies validate our RSTS iPSC-derived neuronal model, because we obtained functional neurons that could be exploited to disclose impairments in cellular excitability of patients' neurons. These results demonstrate the maturation of iPSCs-derivatives into functional neurons expressing sodium and potassium currents, the principal ionic conductances involved in the generation and propagation of action potentials. The small increase in sodium and potassium current densities expressed by neurons from patient #34 may reflect the natural genetic heterogeneity that has been widely reported for cell lines derived from unique individuals, rather than a specific pathological feature (Hu et al., 2010; Adegbola et al., 2017). The observed decreased excitability of patients' neurons may feasibly represent one of the underlying pathological mechanisms leading to the cognitive impairment in RSTS, as it has already been shown for iPSCs-derived neurons of other neurodevelopmental disorders characterized by developmental delay and intellectual disability (Marchetto et al., 2010; Pasca et al., 2011; Mariani et al., 2015). Of interest, the electrophysiological analysis of the intrinsic excitability, which is not directly linked to the morphology of neuronal branches, allowed a more comprehensive characterization of patients' neurons. In fact, neurons of patient #46 show intrinsic hypoexcitable features, although they are morphologically similar to control neurons. In future studies, it will be interesting to investigate whether the observed modifications of neuronal branches lead to an altered synaptic transmission, because features of synaptic transmission are related to dendritic and axonal complexity.

5. Conclusions

The overall results attest that we have generated an in vitro neuronal model of Rubinstein-Taybi syndrome that can be used as a robust in vitro platform to explore the mechanistic basis of this disorder. Morphological changes and decreased excitability of patients' neurons are potential RSTS biomarkers to be further investigated in relation to genotype-dependent RSTS phenotypes. The resource of i-neurons from multiple RSTS patients can be exploited in future studies to provide more detailed insights on correlations between the affected locus, the type of mutation and the cellular phenotype.

Supplementary data to this article can be found online at https://doi.org/10.1016/j.scr.2018.05.019.

Conflict-of interest disclosure

The authors declare no competing financial interests.

Acknowledgments

The authors thank the patients and their families for their participation in this research study and the Italian Association for Rubinstein Taybi “Una vita Speciale” for cooperation. The helpful advice of Prof. S. Chamberlain (Farmington, US) in setting up the iPSC neuronal model is gratefully acknowledged. This work was supported by ERA-NET NEURON JTC2015 ChromiSyn (to LL). The valuable discussion primed by the coordinator of the network Prof. A. Barco (Alicante) has been highly appreciated.

References

Achenbach, T.M., Rescorla, L.A., 2001. In: Frigerio, A. (Ed.), ASEBA University of Vermount (USA), Research Center for Children, Youth and Families. Italian version. Istituto Scientifico E. Medea. Ass La Nostra Famiglia, Bosisio Parini (LC).

Adegbola, A., Bury, L.A., Fu, C., Zhang, M., Wynshaw-Boris, A., 2017. Concise review: induced pluripotent stem cell models for neuropsychiatric diseases. Stem Cells Transl. Med. 6, 2062–2070. http://dx.doi.org/10.1002/sctm.17-0150.

Amps, K., et al., Stem Cell Initiative, 2011. Screening ethnically diverse human embryonic stem cells identifies a chromosome 20 minimal amplicon conferring growth advantage. Nat. Biotechnol. 29, 1132–1144. http://dx.doi.org/10.1038/nbt.2051.

Ardhanareeswaran, K., Mariani, J., Coppola, G., Abyzov, A., Vaccarino, F.M., 2017. Human induced pluripotent stem cells for modelling neurodevelopmental disorders. Nat. Rev. Neurol. 13, 265–278. http://dx.doi.org/10.1038/nrneurol.2017.45.

Arganda-Carreras, I., Fernandez-Gonzalez, R., Munoz-Barrutia, A., Ortiz-De-Solorzano, C., 2010. 3D reconstruction of histological sections: application to mammary gland tissue. Microsc. Res. Tech. 73, 1019–1029. http://dx.doi.org/10.1002/jemt.20829.

Bentivegna, A., Milani, D., Gervasini, C., Castronovo, P., Mottadelli, F., Manzini, S., Colapietro, P., Giordano, L., Atzeri, F., Divizia, M.T., Uzielli, M.L., Neri, G., Bedeschi, M.F., Faravelli, F., Selicorni, A., Larizza, L., 2006. Rubinstein-Taybi Syndrome: spectrum of CREBBP mutations in Italian patients. BMC Med. Genet. 7 (77). http://dx.doi.org/10.1186/1471-2350-7-77.

Berument, S.K., Rutter, M., Lord, C., Pickles, A., Bailey, A., 1999. Autism screening questionnaire: diagnostic validity. Br. J. Psychiatry 175, 444–451.

Bjornsson, H.T., 2015. The Mendelian disorders of the epigenetic machinery. Genome Res. 25, 1473–1481. http://dx.doi.org/10.1101/gr.190629.115.

Chamberlain, S.J., 2016. Disease modelling using human iPSCs. Hum. Mol. Genet. 25, R173–R181. http://dx.doi.org/10.1093/hmg/ddw209.

Dowey, S.N., Huang, X., Chou, B.K., Ye, Z., Cheng, L., 2012. Generation of integration-free human induced pluripotent stem cells from postnatal blood mononuclear cells by plasmid vector expression. Nat. Protoc. 7, 2013–2021. http://dx.doi.org/10.1038/nprot.2012.121.

Fergelot, P., Van Belzen, M., Van Gils, J., Afenjar, A., Armour, C.M., Arveiler, B., Beets, L., Burglen, L., Busa, T., Collet, M., Deforges, J., de Vries, B.B., Dominguez Garrido, E., Dorison, N., Dupont, J., Francannet, C., Garcia-Minaur, S., Gabau Vila, E., Gebre-Medhin, S., Gener Querol, B., Genevieve, D., Gerard, M., Gervasini, C.G., Goldenberg, A., Josifova, D., Lachlan, K., Maas, S., Maranda, B., Moilanen, J.S., Nordgren, A., Parent, P., Rankin, J., Reardon, W., Rio, M., Roume, J., Shaw, A., Smigiel, R., Sojo, A., Solomon, B., Stembalska, A., Stumpel, C., Suarez, F., Terhal, P., Thomas, S., Touraine, R., Verloes, A., Vincent-Delorme, C., Wincent, J., Peters, D.J., Bartsch, O., Larizza, L., Lacombe, D., Hennekam, R.C., 2016. Phenotype and genotype in 52 patients with Rubinstein-Taybi syndrome caused by EP300 mutations. Am. J. Med. Genet. A 170, 3069–3082. http://dx.doi.org/10.1002/ajmg.a.37940.

Germain, N.D., Chen, P.F., Plocik, A.M., Glatt-Deeley, H., Brown, J., Fink, J.J., Bolduc, K.A., Robinson, T.M., Levine, E.S., Reiter, L.T., Graveley, B.R., Lalande, M., Chamberlain, S.J., 2014. Gene expression analysis of human induced pluripotent stem cell-derived neurons carrying copy number variants of chromosome 15q11-

q13.1. Mol. Autism 5, 44. http://dx.doi.org/10.1186/2040-2392-5-44.
Griffiths, R., 1986. The Abilities of Babies: A Study in Mental Measurement. The Test Agency LTD, Cournswood House, North Dean, HighWycombe, Bucks.
Hennekam, R.C., 2006. Rubinstein-Taybi syndrome. Eur. J. Hum. Genet. 14, 981–985. http://dx.doi.org/10.1038/sj.ejhg.5201594.
Howlin, P., Karpf, J., 2004. Using the social communication questionnaire to identify "autistic spectrum" disorders associated with other genetic conditions: findings from a study of individuals with Cohen syndrome. Autism 8, 175–182. http://dx.doi.org/10.1177/1362361304042721.
Hu, B.Y., Weick, J.P., Yu, J., Ma, L.X., Zhang, X.Q., Thomson, J.A., Zhang, S.C., 2010. Neural differentiation of human induced pluripotent stem cells follows developmental principles but with variable potency. Proc. Natl. Acad. Sci. U. S. A. 107, 4335–4340. http://dx.doi.org/10.1073/pnas.0910012107.
Kang, S., Chen, X., Gong, S., Yu, P., Yau, S., Su, Z., Zhou, L., Yu, J., Pan, G., Shi, L., 2017. Characteristic analyses of a neural differentiation model from iPSC-derived neuron according to morphology, physiology, and global gene expression pattern. Sci. Rep. 7 (12233). http://dx.doi.org/10.1038/s41598-017-12452-x.
Kim, D.S., Ross, P.J., Zaslavsky, K., Ellis, J., 2014. Optimizing neuronal differentiation from induced pluripotent stem cells to model ASD. Front. Cell. Neurosci. 8 (109). http://dx.doi.org/10.3389/fncel.2014.00109.
Linda, K., Fiuza, C., Nadif Kasri, N., 2018. The promise of induced pluripotent stem cells for neurodevelopmental disorders. Prog. Neuro-Psychopharmacol. Biol. Psychiatry 84, 382–391. http://dx.doi.org/10.1016/j.pnpbp.2017.11.009.
Lopez-Atalaya, J.P., Gervasini, C., Mottadelli, F., Spena, S., Piccione, M., Scarano, G., Selicorni, A., Barco, A., Larizza, L., 2012. Histone acetylation deficits in lymphoblastoid cell lines from patients with Rubinstein-Taybi syndrome. J. Med. Genet. 49, 66–74. http://dx.doi.org/10.1136/jmedgenet-2011-100354.
Marchetto, M.C., Carromeu, C., Acab, A., Yu, D., Yeo, G.W., Mu, Y., Chen, G., Gage, F.H., Muotri, A.R., 2010. A model for neural development and treatment of Rett syndrome using human induced pluripotent stem cells. Cell 143, 527–539. http://dx.doi.org/10.1016/j.cell.2010.10.016.
Mariani, J., Coppola, G., Zhang, P., Abyzov, A., Provini, L., Tomasini, L., Amenduni, M., Szekely, A., Palejev, D., Wilson, M., Gerstein, M., Grigorenko, E.L., Chawarska, K., Pelphrey, K.A., Howe, J.R., Vaccarino, F.M., 2015. FOXG1-dependent dysregulation of GABA/glutamate neuron differentiation in autism spectrum disorders. Cell 162, 375–390. http://dx.doi.org/10.1016/j.cell.2015.06.034.
Menke, L.A., DDD study, Gardeitchik, T., Hammond, P., Heimdal, K.R., Houge, G., Hufnagel, S.B., Ji, J., Johansson, S., Kant, S.G., Kinning, E., Leon, E.L., Newbury-Ecob, R., Paolacci, S., Pfundt, R., Ragge, N.K., Rinne, T., Ruivenkamp, C., Saitta, S.C., Sun, Y., Tartaglia, M., Terhal, P.A., van Essen, A.J., Vigeland, M.D., Xiao, B., Hennekam, R.C., 2018. Further delineation of an entity caused by CREBBP and EP300 mutations but not resembling Rubinstein-Taybi syndrome. Am. J. Med. Genet. A 176, 862–876. http://dx.doi.org/10.1002/ajmg.a.38626.
Milani, D., Bonarrigo, F.A., Menni, F., Spaccini, L., Gervasini, C., Esposito, S., 2016. Hepatoblastoma in Rubinstein-Taybi syndrome: a case report. Pediatr. Blood Cancer 63, 572–573. http://dx.doi.org/10.1002/pbc.25806.
Mullighan, C.G., Zhang, J., Kasper, L.H., Lerach, S., Payne-Turner, D., Phillips, L.A., Heatley, S.L., Holmfeldt, L., Collins-Underwood, J.R., Ma, J., Buetow, K.H., Pui, C.H., Baker, S.D., Brindle, P.K., Downing, J.R., 2011. CREBBP mutations in relapsed acute lymphoblastic leukaemia. Nature 471, 235–239. http://dx.doi.org/10.1038/nature09727.
Nagy, J., Kobolak, J., Berzsenyi, S., Abraham, Z., Avci, H.X., Bock, I., Bekes, Z., Hodoscsek, B., Chandrasekaran, A., Teglasi, A., Dezso, P., Kovanyi, B., Voros, E.T., Fodor, L., Szel, T., Nemeth, K., Balazs, A., Dinnyes, A., Lendvai, B., Levay, G., Roman, V., 2017. Altered neurite morphology and cholinergic function of induced pluripotent stem cell-derived neurons from a patient with Kleefstra syndrome and autism. Transl. Psychiatry 7, e1179. http://dx.doi.org/10.1038/tp.2017.144.
Negri, G., Magini, P., Milani, D., Colapietro, P., Rusconi, D., Scarano, E., Bonati, M.T., Priolo, M., Crippa, M., Mazzanti, L., Wischmeijer, A., Tamburrino, F., Pippucci, T., Finelli, P., Larizza, L., Gervasini, C., 2016. From whole gene deletion to point mutations of EP300-positive Rubinstein-Taybi patients: new insights into the mutational spectrum and peculiar clinical hallmarks. Hum. Mutat. 37, 175–183. http://dx.doi.org/10.1002/humu.22922.
Park, E., Kim, Y., Ryu, H., Kowall, N.W., Lee, J., Ryu, H., 2014. Epigenetic mechanisms of Rubinstein-Taybi syndrome. NeuroMolecular Med. 16, 16–24. http://dx.doi.org/10.1007/s12017-013-8285-3.
Pasca, S.P., Portmann, T., Voineagu, I., Yazawa, M., Shcheglovitov, A., Pasca, A.M., Cord, B., Palmer, T.D., Chikahisa, S., Nishino, S., Bernstein, J.A., Hallmayer, J., Geschwind, D.H., Dolmetsch, R.E., 2011. Using iPSC-derived neurons to uncover cellular phenotypes associated with Timothy syndrome. Nat. Med. 17, 1657–1662. http://dx.doi.org/10.1038/nm.2576.
Roid, G.H., Miller, L.J., 1997. Leiter international performance scale-revised: examiner's manual. In: Roid, G.H., Miller, L.J. (Eds.), Leiter International Performance Scale-Revised. Stoelting Co., Wood Dale, IL, USA.
Rutter, M., Bailey, A., Lord, C., Berument, S.K., 2003. The Social Communication Questionnaire. Western Psychological Services, Los Angeles.
Schlaeger, T.M., Daheron, L., Brickler, T.R., Entwisle, S., Chan, K., Cianci, A., DeVine, A., Ettenger, A., Fitzgerald, K., Godfrey, M., Gupta, D., McPherson, J., Malwadkar, P., Gupta, M., Bell, B., Doi, A., Jung, N., Li, X., Lynes, M.S., Brookes, E., Cherry, A.B., Demirbas, D., Tsankov, A.M., Zon, L.I., Rubin, L.L., Feinberg, A.P., Meissner, A., Cowan, C.A., Daley, G.Q., 2015. A comparison of non-integrating reprogramming methods. Nat. Biotechnol. 33, 58–63. http://dx.doi.org/10.1038/nbt.3070.
Soares, F.A., Pedersen, R.A., Vallier, L., 2016. Generation of human induced pluripotent stem cells from peripheral blood mononuclear cells using Sendai virus. Methods Mol. Biol. 1357, 23–31. http://dx.doi.org/10.1007/7651_2015_202.
Spena, S., Milani, D., Rusconi, D., Negri, G., Colapietro, P., Elcioglu, N., Bedeschi, F., Pilotta, A., Spaccini, L., Ficcadenti, A., Magnani, C., Scarano, G., Selicorni, A., Larizza, L., Gervasini, C., 2015. Insights into genotype-phenotype correlations from CREBBP point mutation screening in a cohort of 46 Rubinstein-Taybi syndrome patients. Clin. Genet. 88, 431–440. http://dx.doi.org/10.1111/cge.12537.
Takahashi, K., Tanabe, K., Ohnuki, M., Narita, M., Ichisaka, T., Tomoda, K., Yamanaka, S., 2007. Induction of pluripotent stem cells from adult human fibroblasts by defined factors. Cell 131, 861–872. http://dx.doi.org/10.1016/j.cell.2007.11.019.
Terragni, B., Scalmani, P., Colombo, E., Franceschetti, S., Mantegazza, M., 2016. Ranolazine vs phenytoin: greater effect of ranolazine on the transient Na(+) current than on the persistent Na(+) current in central neurons. Neuropharmacology 110, 223–236. http://dx.doi.org/10.1016/j.neuropharm.2016.06.029.
Valor, L.M., Pulopulos, M.M., Jimenez-Minchan, M., Olivares, R., Lutz, B., Barco, A., 2011. Ablation of CBP in forebrain principal neurons causes modest memory and transcriptional defects and a dramatic reduction of histone acetylation but does not affect cell viability. J. Neurosci. 31, 1652–1663. http://dx.doi.org/10.1523/JNEUROSCI.4737-10.2011.
Verpelli, C., Carlessi, L., Bechi, G., Fusar Poli, E., Orellana, D., Heise, C., Franceschetti, S., Mantegazza, R., Mantegazza, M., Delia, D., Sala, C., 2013. Comparative neuronal differentiation of self-renewing neural progenitor cell lines obtained from human induced pluripotent stem cells. Front. Cell. Neurosci. 7 (175). http://dx.doi.org/10.3389/fncel.2013.00175.
Wang, J., Weaver, I.C., Gauthier-Fisher, A., Wang, H., He, L., Yeomans, J., Wondisford, F., Kaplan, D.R., Miller, F.D., 2010. CBP histone acetyltransferase activity regulates embryonic neural differentiation in the normal and Rubinstein-Taybi syndrome brain. Dev. Cell 18, 114–125. http://dx.doi.org/10.1016/j.devcel.2009.10.023.